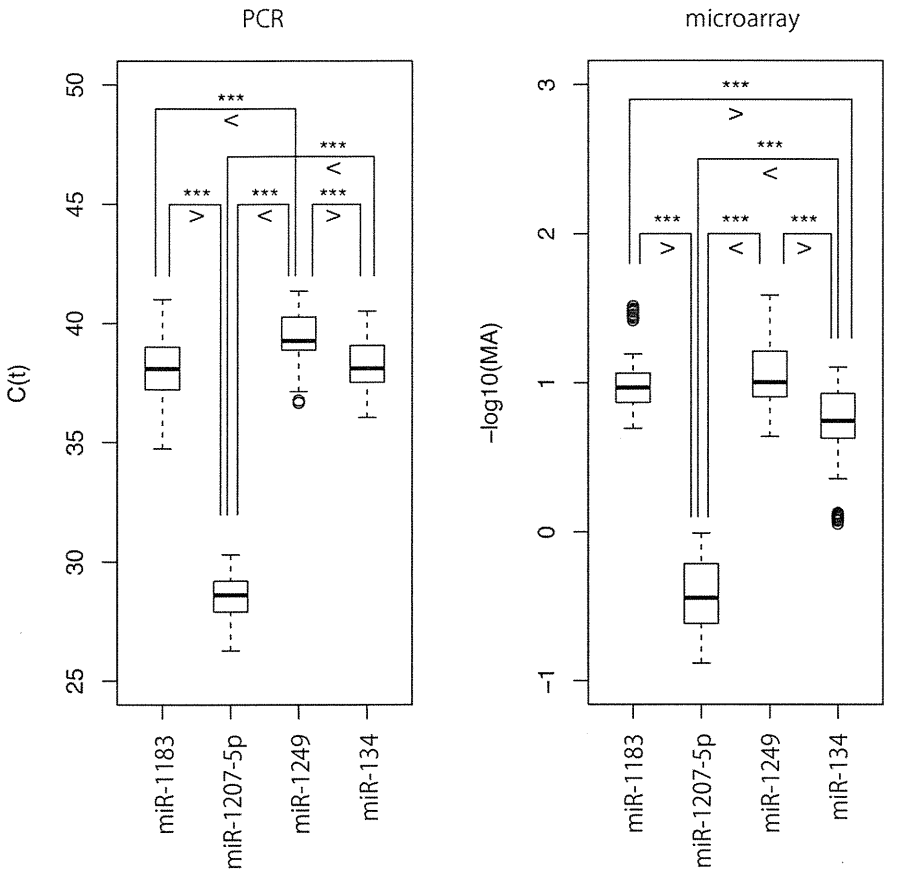

Figure 8. Real-time qPCR validation of microarray analysis. The microarray expression analysis result of four miRNAs was reproduced in real-time PCR analysis. The pairs with $p<0.001$ are marked by "***".
doi:10.1371/journal.pone.0048366.g008

All reactions were run in triplicate. Chromo 4 detector (Bio-rad) was used to detect miRNA expression. To allow for the validation of microarray results with C(t) obtained by qPCR, raw gene expressions were transformed into logarithmic values. P-values were computed via one-sided t test. No averages over probes were taken for the microarray. The above procedures were also done with various packages/functions implemented in R (http://www.r-project.org/).

Statistical Analysis

For symptoms having discrete values, grade pairs were compared with Wilcoxon rank sum test (one-sided); otherwise, P-values were computed from correlation coefficients. In both cases, false discovery rate (FDR) of less then 0.05 computed from the P-value was regarded as significant. Benjamini and Hochberg criterion was used for FDR estimation. All p-values shown are significant even though they are raw numbers. No average over probes was taken before correlation analyses.

The Canonical Correlation Coefficients for miRNA Expression and Clinical Parameters

The canonical correlation coefficients were computed for ALT-miRNA, albumin-miRNA, and HCVRNA-miRNA correlations, using up to 12 miRNA with larger correlation coefficients (see Supporting Information).

Classification Analyses for Liver Fibrosis/inflammation

P-values were computed via one-sided t test using the raw expression values of each miRNA from the samples of CHC and healthy controls. The logarithm of obtained P-values was then transformed into principal components scores via principal components analysis. Following this, grades were discriminated by linear discriminant analysis of CHC ages and the optimal number of principal components.

Selection of miRNAs Required to Diagnose Several Liver Diseases

For specific pairs consisting of one liver disease and a healthy control, their normalized miRNAs expression was transformed into principal components scores via principal components analysis. miRNAs having the larger first and second principal component scores were selected. Following this, the principal component scores of each sample was computed based solely on the selected miRNA expressions. Liver diseases were classified using the optimal number of these principal component scores.

In order to compensate for the relative small number of NASH and CHB patients, we performed "*in silico*" patients resampling analysis of the microarray data (see Supporting Information). All the above procedures were done with various packages/functions implemented in R.

"*In silico*" Resampling

"*In silico*" resampling is a tool often used to overcome the limitation of a small sample size. Using this technique, we combined the clinical traits of existing patients and created various virtual samples. Using these virtual cohorts, we were then able to increase the sample size (see Supporting information).

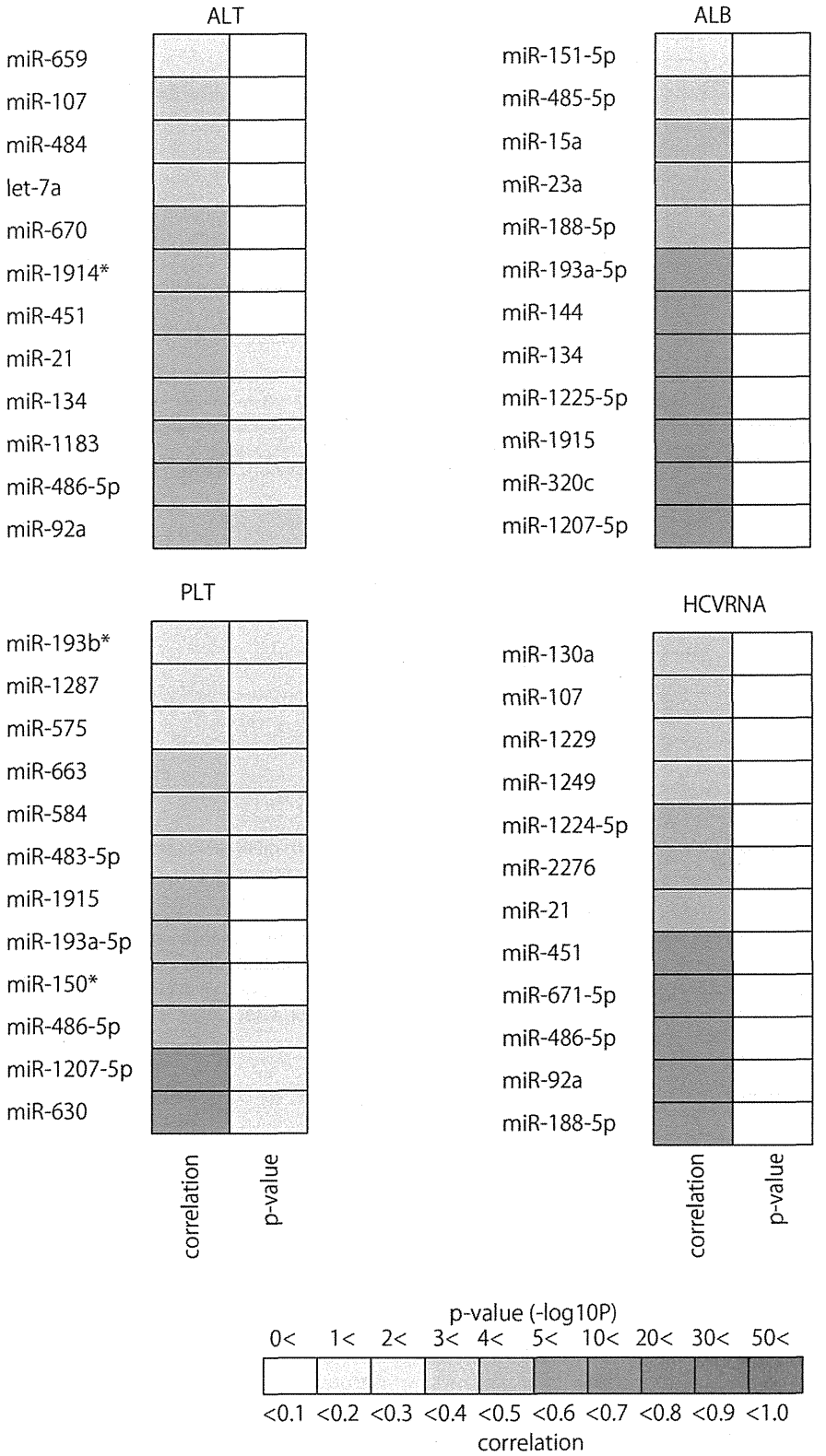

Figure 9. The list of miRNAs used to obtain the maximum correlation coefficient between miRNA expression level, and clinical characteristics. Pairwise heatmap showing miRNAs and their correlation coefficient and p-values.
doi:10.1371/journal.pone.0048366.g009

In order to validate the *"in silico"* resampling results, we prepared another sample set and once again performed *"in silico"* resampling using the microarray data from 99 CHC liver tissue samples [36]. The results proved that "*in silico*" resampling can accurately reproduce an entire population using only a small number of existing samples (see Supporting Information).

Reproducibility Test of Microarray Data

Data were analyzed using the GeneSpring GX10.0.2 (Agilent). Quality control (QC) was applied according to the manufacturer's instructions, and all data were approved by GeneSpring. Following Agilent recommendations, no inter-array normalization was applied because the similarity in miRNA expression among sample arrays was unknown [37]. Scatter plots and Pearson's pairwise correlations were performed with GeneSpring.

Supporting Information

Figure S1 Expression patterns of miRNAs used for discriminating among CHC, NL, CHB, and NASH. Classifying CHC, NL, CHB, and NASH using LOOCV. Distinguishing between two arbitrary groups using LOOCV.
(TIF)

Figure S2 Expression patterns of miRNAs used to discriminate among CHC, CHB, NASH, and NL "in silico" resampling for disease discriminant studies reflected by BMI. A. Box plots of expression pattern of the miRNAs used to discriminate among CHC, CHB, NASH, and NL. B. Discriminating among four groups using LOOCV. Accuracy is 95.25%. C. Two dimensional embedding of CHC, CHB, NASH, and NL by the first and second principle component scores computed with 12 selected miRNAs
(TIF)

Figure S3 The same as Fig.3 for CHC and CHB. A. Box plot of 19 miRNAs used for the discrimination. B. Classification between CHC and CHB. Accuracy is 100%. C. The two dimensional embedding of CHB and CHC by the first and second principal component scores computed with19 selected miRNAs.
(TIF)

Figure S4 The same as Fig.S3 for CHC and NASH. A. Box plots of 20 miRNAs used for the discrimination. B. Classification between CHC and NASH. Accuracy is 100%. C. Two dimensional embedding of CHC and NASH by the first and second principal component scores computed with 19 selected miRNAs
(TIF)

Figure S5 The same as Fig.S3 for CHC and NL. A. Box plots of 9 miRNAs used for the discrimination. B. Classification between CHC and NL. Accuracy is 100%. C. Two dimensional embedding of CHC and NL by the first and second principal component scores computed with 9 selected miRNAs
(TIF)

Figure S6 The same as Fig.S3 for CHB and NL. A. Box plots of 4 miRNAs used for the discrimination. B. Classification between CHB and NL. Accuracy is 93.5%. C. Two dimensional embedding of CHB and NL by the first and second principal component scores computed with 4 selected miRNAs
(TIF)

Figure S7 The same as Fig.S3 for NASH and NL. A. Box plots of 5 miRNAs used for the discrimination. B. Distinguishing between NASH and NL with 84.0% accuracy. C. Two dimensional embedding of NASH and NL by the first and second principal component scores computed with 5 selected miRNAs
(TIF)

Figure S8 The same as Fig.S3 for CHB and NASH pair. A. Box plots of 17 miRNAs used for the discrimination. B. Distinguishing between CHB and NASH with 80.0% accuracy. C. Two dimensional embedding of CHB and NASH by the first and second principal component scores computed with 17 selected miRNAs
(TIF)

Figure S9 Classification of the independent sample using semi-supervised learning based on the labels in the original cohort. A. Classifying CHB and CHC. Accuracy is 74.47%. B. Classifying CHC and NASH. Accuracy is 87.18%. C. Classifying CHB and NASH. Accuracy is 79.19%.
(TIF)

Figure S10 miRNA expression pattern that correlated with the changes in clinical background. miRNAs that were differentially expressed according to the grade of liver inflammation
(TIF)

Figure S11 miRNA expression pattern that correlated with the changes in clinical background. miRNAs that were differentially expressed according to liver fibrosis stage
(TIF)

Figure S12 Real-time qPCR validation of microarray analysis "in silico" resampling for disease discrimination studies reflected by BMI. The result of microarray expression analysis of four miRNAs was reproduced using real-time PCR analysis. Pairs with $p<0.001$ are marked by "***".
(TIF)

Figure S13 The relationship between the expression levels of several miRNAs and serum ALT, albumin, HCVRNA, respectively. Horizontal axis shows the number of miRNAs used in the analysis. Vertical axis shows the correlation index and p-values.
(TIF)

Figure S14 Summary of the relationship between the expression level of miR-122 and several clinical features. A. Expression level of miR-122 positively correlated with an increase in liver inflammatory grade. Asterisk denotes significant differences of $p<0.05$. B. Expression level of miR-122 positively correlated with the serum level of albumin. C. Expression level of miR-122 positively correlated with the amount of serum HCVRNA. D. Expression level of miR-122 in exosome rich fraction did not significantly correlate with that in liver tissues.
(TIF)

Table S1 The list of miRNAs used for classifying arbitrary 2 groups and 4 groups, and their p-values.
(DOCX)

Table S2 Significantly differentially expressed miRNAs according liver inflammation grade and liver fibrotic stage.
(DOCX)

Table S3 The list of miRNAs used to obtain the maximum correlation coefficient between expression level of miRNAs, and clinical characteristics.
(DOCX)

Table S4 List of miRNAs with expression that corresponded in liver tissue and serum.
(DOCX)

Table S5 Clinical background of original samples and independent samples in detail.
(DOCX)

Table S6 Accuracy of LDA for "in silico" resampling.
(DOCX)

Supplemental Information
(DOCX)

Author Contributions

Conceived and designed the experiments: YM NK TO YT. Performed the experiments: YM HT TT YY NK. Analyzed the data: TT YT. Contributed reagents/materials/analysis tools: HT JT TK. Wrote the paper: YM NK TO.

References

1. Ambros V (2004) The functions of animal microRNAs. Nature 431: 350–355.
2. Murakami Y, Toyoda H, Tanaka M, Kuroda M, Harada Y, et al. (2011) The progression of liver fibrosis is related with overexpression of the miR-199 and 200 families. PLoS One 6: e16081.
3. Murakami Y, Yasuda T, Saigo K, Urashima T, Toyoda H, et al. (2006) Comprehensive analysis of microRNA expression patterns in hepatocellular carcinoma and non-tumorous tissues. Oncogene 25: 2537–2545.
4. Braconi C, Henry JC, Kogure T, Schmittgen T, Patel T (2011) The role of microRNAs in human liver cancers. Semin Oncol 38: 752–763.
5. Hsu SH, Wang B, Kota J, Yu J, Costinean S, et al. (2012) Essential metabolic, anti-inflammatory, and anti-tumorigenic functions of miR-122 in liver. J Clin Invest 122: 2871–2883.
6. Tsai WC, Hsu SD, Hsu CS, Lai TC, Chen SJ, et al. (2012) MicroRNA-122 plays a critical role in liver homeostasis and hepatocarcinogenesis. J Clin Invest 122: 2884–2897.
7. Valadi H, Ekstrom K, Bossios A, Sjostrand M, Lee JJ, et al. (2007) Exosome-mediated transfer of mRNAs and microRNAs is a novel mechanism of genetic exchange between cells. Nat Cell Biol 9: 654–659.
8. Kosaka N, Iguchi H, Yoshioka Y, Takeshita F, Matsuki Y, et al. (2010) Secretory mechanisms and intercellular transfer of microRNAs in living cells. J Biol Chem 285: 17442–17452.
9. Zhang Y, Liu D, Chen X, Li J, Li L, et al. (2010) Secreted monocytic miR-150 enhances targeted endothelial cell migration. Mol Cell 39: 133–144.
10. Pegtel DM, Cosmopoulos K, Thorley-Lawson DA, van Eijndhoven MA, Hopmans ES, et al. (2010) Functional delivery of viral miRNAs via exosomes. Proc Natl Acad Sci U S A 107: 6328–6333.
11. Kogure T, Lin WL, Yan IK, Braconi C, Patel T (2011) Intercellular nanovesicle-mediated microRNA transfer: a mechanism of environmental modulation of hepatocellular cancer cell growth. Hepatology 54: 1237–1248.
12. Thery C, Ostrowski M, Segura E (2009) Membrane vesicles as conveyors of immune responses. Nat Rev Immunol 9: 581–593.
13. Mittelbrunn M, Gutierrez-Vazquez C, Villarroya-Beltri C, Gonzalez S, Sanchez-Cabo F, et al. (2011) Unidirectional transfer of microRNA-loaded exosomes from T cells to antigen-presenting cells. Nat Commun 2: 282.
14. Meckes DG Jr, Shair KH, Marquitz AR, Kung CP, Edwards RH, et al. (2010) Human tumor virus utilizes exosomes for intercellular communication. Proc Natl Acad Sci U S A 107: 20370–20375.
15. Gould SJ, Booth AM, Hildreth JE (2003) The Trojan exosome hypothesis. Proc Natl Acad Sci U S A 100: 10592–10597.
16. Kosaka N, Iguchi H, Ochiya T (2010) Circulating microRNA in body fluid: a new potential biomarker for cancer diagnosis and prognosis. Cancer Sci 101: 2087–2092.
17. Mitchell PS, Parkin RK, Kroh EM, Fritz BR, Wyman SK, et al. (2008) Circulating microRNAs as stable blood-based markers for cancer detection. Proc Natl Acad Sci U S A 105: 10513–10518.
18. Chen X, Ba Y, Ma L, Cai X, Yin Y, et al. (2008) Characterization of microRNAs in serum: a novel class of biomarkers for diagnosis of cancer and other diseases. Cell Res 18: 997–1006.
19. Lawrie CH (2007) MicroRNAs and haematology: small molecules, big function. Br J Haematol 137: 503–512.
20. Cermelli S, Ruggieri A, Marrero JA, Ioannou GN, Beretta L (2011) Circulating microRNAs in patients with chronic hepatitis C and non-alcoholic fatty liver disease. PLoS One 6: e23937.
21. Bihrer V, Friedrich-Rust M, Kronenberger B, Forestier N, Haupenthal J, et al. (2011) Serum miR-122 as a biomarker of necroinflammation in patients with chronic hepatitis C virus infection. Am J Gastroenterol 106: 1663–1669.
22. Ji F, Yang B, Peng X, Ding H, You H, et al. (2011) Circulating microRNAs in hepatitis B virus-infected patients. J Viral Hepat 18: e242–251.
23. Starkey Lewis PJ, Dear J, Platt V, Simpson KJ, Craig DG, et al. (2011) Circulating microRNAs as potential markers of human drug-induced liver injury. Hepatology 54: 1767–1776.
24. Chapelle O, Scholkopf B, Zien A (2006) Semi-supervised learning. Cambridge, Mass.: MIT Press. x, 508 p. p.
25. Hunter MP, Ismail N, Zhang X, Aguda BD, Lee EJ, et al. (2008) Detection of microRNA expression in human peripheral blood microvesicles. PLoS One 3: e3694.
26. Marquez RT, Bandyopadhyay S, Wendlandt EB, Keck K, Hoffer BA, et al. (2010) Correlation between microRNA expression levels and clinical parameters associated with chronic hepatitis C viral infection in humans. Lab Invest 90: 1727–1736.
27. Mathivanan S, Ji H, Simpson RJ (2010) Exosomes: extracellular organelles important in intercellular communication. J Proteomics 73: 1907–1920.
28. Simons M, Raposo G (2009) Exosomes–vesicular carriers for intercellular communication. Curr Opin Cell Biol 21: 575–581.
29. Keller A, Leidinger P, Bauer A, Elsharawy A, Haas J, et al. (2011) Toward the blood-borne miRNome of human diseases. Nat Methods 8: 841–843.
30. Laterza OF, Lim L, Garrett-Engele PW, Vlasakova K, Muniappa N, et al. (2009) Plasma MicroRNAs as sensitive and specific biomarkers of tissue injury. Clin Chem 55: 1977–1983.
31. Nathwani RA, Pais S, Reynolds TB, Kaplowitz N (2005) Serum alanine aminotransferase in skeletal muscle diseases. Hepatology 41: 380–382.
32. Landgraf P, Rusu M, Sheridan R, Sewer A, Iovino N, et al. (2007) A mammalian microRNA expression atlas based on small RNA library sequencing. Cell 129: 1401–1414.
33. Dowman JK, Tomlinson JW, Newsome PN (2011) Systematic review: the diagnosis and staging of non-alcoholic fatty liver disease and non-alcoholic steatohepatitis. Aliment Pharmacol Ther 33: 525–540.
34. Bedossa P, Poynard T (1996) An algorithm for the grading of activity in chronic hepatitis C. The METAVIR Cooperative Study Group. Hepatology 24: 289–293.
35. Matteoni CA, Younossi ZM, Gramlich T, Boparai N, Liu YC, et al. (1999) Nonalcoholic fatty liver disease: a spectrum of clinical and pathological severity. Gastroenterology 116: 1413–1419.
36. Murakami Y, Tanaka M, Toyoda H, Hayashi K, Kuroda M, et al. (2010) Hepatic microRNA expression is associated with the response to interferon treatment of chronic hepatitis C. BMC Med Genomics 3: 48.
37. Zhang X, Chen J, Radcliffe T, Lebrun DP, Tron VA, et al. (2008) An array-based analysis of microRNA expression comparing matched frozen and formalin-fixed paraffin-embedded human tissue samples. J Mol Diagn 10: 513–519.

SCIENTIFIC REPORTS

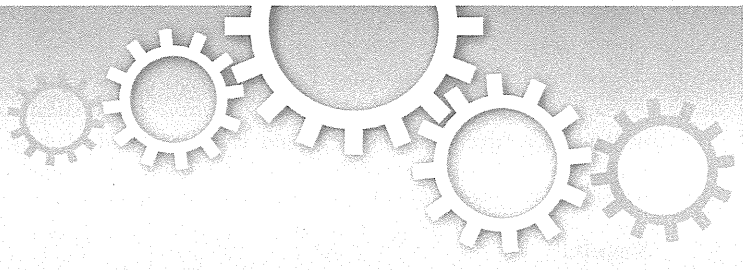

OPEN

SUBJECT AREAS:
PLURIPOTENCY
EMBRYONIC STEM CELLS
CANCER MODELS
MECHANISMS OF DISEASE

Received
17 July 2012

Accepted
29 October 2012

Published
10 December 2012

Correspondence and requests for materials should be addressed to T.O. (tochiya@ncc.go.jp)

Two distinct knockout approaches highlight a critical role for p53 in rat development

Masaki Kawamata & Takahiro Ochiya

Division of Molecular and Cellular Medicine, National Cancer Center Research Institute, 1-1, Tsukiji, 5-chome, Chuo-ku, Tokyo 104-0045, Japan.

Gene targeting in embryonic stem cells (ESCs) has become the principal technology for generating knockout models. Although numerous studies have predicted that the disruption of *p53* leads to increased developmental anomalies and malignancies, most *p53* knockout mice develop normally. Therefore, the role of *p53* in animal development was examined using rat knockout models. Conventionally generated homozygous KO males developed normally, whereas females rarely survived due to neural tube defects. Mutant chimeras generated via blastocyst injection with *p53*-null ESCs exhibited high rates of embryonic lethality in both sexes. This phenotype could be observed in one month by the use of zinc-finger nucleases. The *p53*-null ESCs were resistant to apoptosis and differentiation, and exhibited severe chromosome instabilities in the chimera-contributed cells, suggesting an essential role for p53 in maintaining ESC quality and genomic integrity. These results demonstrate that p53 functions as a guardian of embryogenesis in the rats.

Over the past two decades, knockout (KO) technology in mice has helped to clarify the physiological function of a large number of genes. However, unexpected phenotypes have been observed in some cases, making it difficult to understand the role of the deleted gene, or to translate that data to the phenotypes of human diseases caused by mutations in such genes. Thus, gene-targeting techniques for other animals, such as rats, have long been sought. Many strategies for manipulating rat genes to generate loss-of-function models have been adapted from the mouse genetic toolbox, including conventional transgenesis by pronuclear injection[1], RNA interference[2], N-ethyl-N-nitrosourea (ENU) mutagenesis[3,4], and transposon mutagenesis[5–7]. KO rats have been produced using Zinc-finger nuclease (ZFN) technology[8,9], and, most recently, germline-competent rat ESCs and rat induced pluripotent stem cells (iPSCs) have been established by the addition of cell-signaling inhibitors to the culture medium[10–13], making it possible to generate both transgenic (Tg)[12,14] and KO rats[15].

The tumor suppressor gene *p53* is a good example of a gene whose function in mouse development requires further scrutiny. Donehower et al. first reported normal Mendelian ratios and postnatal development in *p53* homozygous KO mice[16]. However, two other groups later showed that a fraction of homozygous KO females had fatal embryonic exencephaly, a defect in neural tube closure that results in an overgrowth of neural tissue in the midbrain region[17,18]. Such results indicate that, at least in some cases, p53 influences development in females[19]. In the case of *p53* homozygous KO rats, neural tube defects (NTDs) in females were not found but increased susceptibility to tumor development was reported[15,20,21].

p53 has been shown to regulate not only cell cycle arrest, apoptosis, and DNA repair in many types of cells[22], but also stemness, by suppressing *Nanog* expression in ESCs[23]. Considering these observations, malignant transformations may occur in *p53*-null ESCs and chimera development may be hindered. However, chimeric mutant mice have been successfully generated via the injection of blastocysts with iPSCs derived from *p53*-null mouse embryonic fibroblasts (MEFs), and germline transmission of the *p53*-null cells was also accomplished[24,25]. The properties of rat ESCs differ from those of mouse ESCs in that rat ESCs cannot be cultured in mouse ESC culture conditions due to their high sensitivity to differentiation signals[26]. Thus, an approach using *p53*-null rat ESCs might reveal new insights into the function of p53 in regulating stemness and animal development.

We previously generated *Oct4*-Venus Tg rats, and established *Oct4*-Venus ESC lines in which *Oct4* expression can be monitored by green fluorescence[12,27]. Here, both conventionally KO and mutant chimeras rats were generated using *p53*-null *Oct4*-Venus ESCs, and their development was investigated. Moreover, an efficient

method for a rapid generation of mutant chimeras was developed using ZFN-mediated gene targeting in rat ESCs. Using this method, developmental phenotypes can be observed within 1 month.

Results

Conventionally generated $p53^{-/-}$ females reveal the cause of NTDs. *p53* homozygous KO rats were generated via germline transmission of heterozygous $p53^{+/C}$ ESCs (Fig. 1a,b,e). The details are described in the *Materials and Methods*. The Mendelian ratios in weaned rats produced from heterozygous intercrosses were investigated (Fig. 2a). The frequency of homozygous $p53^{C/C}$ rats was 16.9%, less than the anticipated value of 25% (Table 1). Moreover, only one $p53^{C/C}$ female developed normally, frequency = 0.70%, significantly less than 16.2% $p53^{C/C}$ males. These results suggest that most of the $p53^{C/C}$ females either do not survive gestation, or die after birth but prior to weaning. To investigate the developmental dysfunctions in $p53^{C/C}$ females, litters from heterozygous intercrosses were examined at embryonic day 16.0 (E16.0) to E18.0. Eleven $p53^{C/C}$ female embryos (12.8%, 11/86) were recovered at this stage; six (57%, 6/11) exhibited exencephaly (Table 1) and two of these also exhibited spina bifida (Fig. 2b). Although these two abnormalities are the most prevalent NTDs, spina bifida in *p53* mutant mice has only been reported in one study[28]. Exencephaly was only found in the female embryos, consistent with previous observations of a higher incidence of NTDs in human females and in numerous mouse models[29]. Expression of SOX2, a marker for primordial neuronal cells

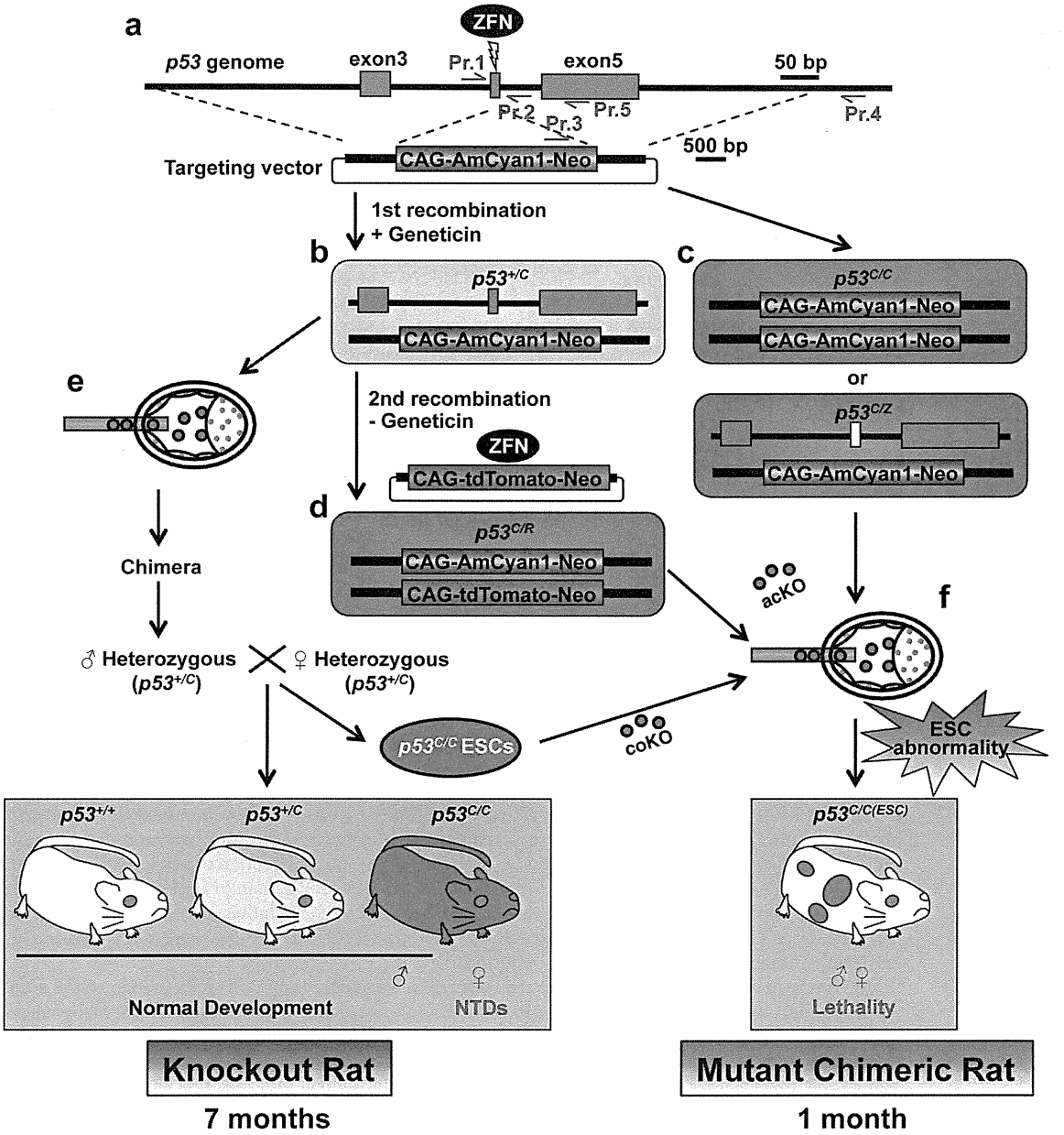

Figure 1 | Schematic representation of *p53* KO strategy in rats. (a–d) Both mono- (b) and bi-allelic (c) or 2ndary (d) homologous recombination are induced by ZFN. (e, f) Heterozygous or homozygous ESC-injection leads to the generation of conventionally generated KO model (e) or ESC-based mutant chimeric models (f), respectively. A yellow box indicates a frame shift mutation induced by ZFNs. Pr., Primer. coKO, congenital KO. acKO, acquired KO.

Table 1 | The *p53* Genotypes of Adult and Embryonic Rats

Genotype	$p53^{+/+}$	$p53^{+/C}$	$p53^{C/C}$	$p53^{C/C}$ Exencephaly
Adults	41 (28.9%)	77 (54.2%)	24 (16.9%)	0
Male	18 (12.7%)	42 (29.6%)	23 (16.2%)	0
Female	23 (16.2%)	35 (24.6%)	1 (0.70%)	0
Embryos	21 (24.4%)	48 (55.8%)	17 (19.8%)	6
Male	11 (12.8%)	22 (25.6%)	6 (7.0%)	0
Female	10 (11.6%)	26 (30.2%)	11 (12.8%)	6 (54.5%)[a]

[a]Of the 11 $p53^{C/C}$ female embryos, six exhibited exencephaly.

expressed in the embryonic neural plate[30], was detected on the surface of the brain and in areas of spina bifida (Fig. 2d, arrowheads), confirming that neural tube closure had failed. Compared to a $p53^{+/C}$ embryo (Fig. 2e, right), the aberrant ventricular zone (VZ) structure in the brain of a $p53^{C/C}$ exencephalic embryo was revealed by the localization of SOX2 (Fig. 2d left, arrows), which is expressed in the neuroendothelial stem cells of the VZ[31]. In this embryo, *Oct4*-Venus expressing cells were aberrantly located in the exencephalic region (Fig. 2b, green square, and 2c).

Embryonic lethality in a mutant chimeric model. ZFNs can create site-specific double-strand breaks, which are repaired via non-homologous end joining, resulting in frame-shift mutations by the arbitrary addition or deletion of base pairs. Cotransfection of ZFNs with targeting vectors enhances homologous recombination, not only in human pluripotent cells[32,33], but also in one-cell embryos, leading to the direct generation of knock-in mice[34] and rats[35]. In the present work, ZFNs were used to produce homozygous mutant ESC lines by a single recombination step (Fig. 1c). Using this approach, 1 of 46 (2.2%) clones harbored dual knock-in alleles ($p53^{C/C}$), while 7 of 46 (15%) clones possessed both knock-in and frame shift mutant alleles ($p53^{C/Z}$). In a 2nd-step recombination, homozygous clones were also produced from a $p53^{+/C3}$ ESC clone based on the same strategy using both ZFNs and a targeting vector expressing red fluorescence (Fig. 1b,d). A successful homologous recombination was achieved in 3 of 8 clones (38%, $p53^{C/R}$; Supplementary Fig. S2c). These ESC lines were called acquired KO (acKO) ESCs (Fig. 1c). The contribution of $p53^{-/-}$ ($p53^{C/C}$, $p53^{C/Z}$, or $p53^{C/R}$) ESCs to rats, which are called $p53^{-/-\,(ESC)}$ rats, was examined, and the timeline for the rapid generation of the mutant chimeras is shown schematically (Fig. 3a,b). Microinjection of $p53^{-/-}$ ESCs into blastocysts led to the delivery of only a few pups (0.4 ± 0.2 per foster mother, n=5, 4 cell lines). This number (0.4 ± 0.2/foster mother) was significantly smaller than the number of pups delivered following injection of $p53^{+/+}$ ESCs into blastocysts (4.0 ± 1.1 per foster mother, n=5, 3 cell lines, $P<0.05$) or $p53^{+/-}$ ($p53^{+/C}$) ESCs (5.1 ± 1.1 per foster mother, n=9, 4 cell lines, $P<0.05$) (Fig. 3c). The

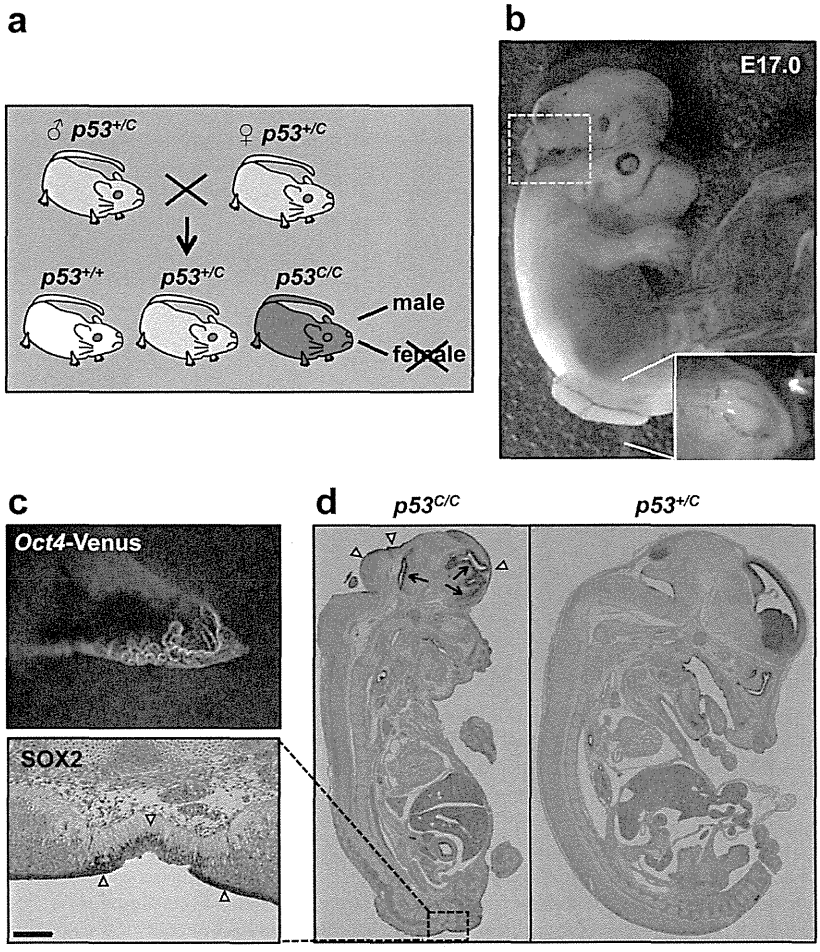

Figure 2 | Phenotypes in conventionally generated p53 homozygous rats. (a) Schematic representation of heterozygous intercrosses indicates a loss of adult female. (b) An embryo at day 17.0 of gestation (E17.0) displaying exencephaly and spina bifida. A dotted green square indicates (c). (c) Fluorescence image of the area inside the dotted green square in (b). *Oct4*-Venus fluorescence is observed in the exencephalic region. (d) IHC staining for SOX2 identifies positive cells in the ventricular zone (arrows) and surface (arrowheads) of both brain and spina bifida (magnified image, scale bar = 100 μm).

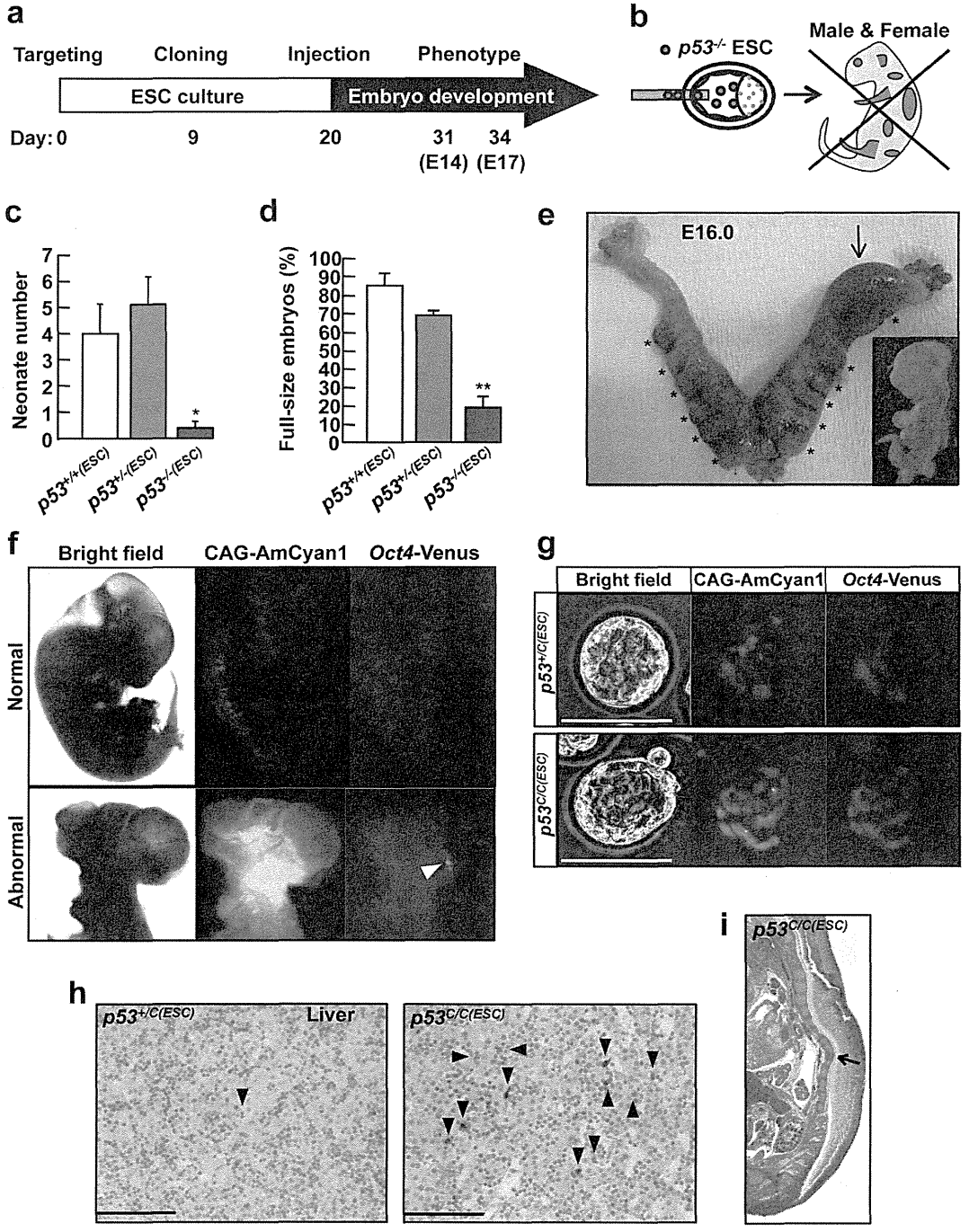

Figure 3 | Embryonic lethality in p53 mutant chimeras. (a) Time line for generating $p53^{-/-(ESC)}$ chimeras and (b) Schematic representation to investigate phenotype during embryogenesis. (c) Number of neonates successfully delivered. $p53^{+/+}$ (n=5, 3 cell lines), $p53^{+/-}$ (n=9, 4 cell lines) or $p53^{-/-}$ (n=5, 4 cell lines) ESCs were injected into wild-type blastocysts. n, injection number. *, $P<0.05$, $p53^{-/-}$ vs. $p53^{+/+}$ and $p53^{+/-}$. (d) The ratio of chimeric embryos with normal body size at E14.0 to E17.0. $p53^{+/+}$ (n=4, 4 cell lines), $p53^{+/-}$ (n=7, 4 cell lines) or $p53^{-/-}$ (n=14, five cell lines) ESCs were injected into wild-type blastocysts. n, injection number. **, $P<0.001$, $p53^{-/-}$ vs. $p53^{+/+}$ and $p53^{+/-}$. (e) Developmental dysfunction in chimeric embryos injected with $p53^{C/R2}$ ESCs at E16.0. An arrow indicates a chimera with growth retardation (inset). Asterisks indicate fetal absorption. (f) Correlation between developmental dysfunction and ESC contribution. $p53^{C/C1}$ ESCs expressing AmCyan1 contribute to chimeric embryos at E14.0. An arrowhead indicates an ectopic expression of *Oct4*-Venus. (g) $p53^{C/R4}$ ESC proliferation in blastocyst. Twelve ESCs were injected into blastocyst, followed by incubation overnight in YPAC medium. (h) Immunohistochemistry using Cleaved-Caspase3 antibody in liver of $p53^{+/C(ESC)}$ or $p53^{C/C(ESC)}$ chimera. Arrowheads indicate the apoptotic cells. (i) Spinal curvature (an arrow) in $p53^{C/C(ESC)}$ chimera. All scale bars = 100 μm.

newborns derived from $p53^{-/-}$ ESC-injections did not exhibit a brown coat-color, indicating that they were not chimeras. Because these results suggest that the development of $p53^{-/-(ESC)}$ embryos was defective, fetal development at stages E14.0 to E17.0 was examined. Approximately 80% of the $p53^{-/-(ESC)}$ embryos (n=14, 5 cell lines, Fig. 3d) showed abnormal development resulting in complete

resorption (Fig. 3e, asterisks) or growth retardation (Fig. 3e, an arrow and inset). A large number of $p53^{-/-}$ ESC-derived cells were detected in these embryos (Fig. 3f, lower). However, the remaining $p53^{-/-\,(ESC)}$ embryos (30/189 embryos: 20.0 ± 5.6%) developed a normal body size (Fig. 3f, upper and Supplementary Table S1). The number of normal embryos (20.0 ± 5.6%) was significantly lower than that of $p53^{+/+(ESC)}$ embryos (53/63 embryos: 85.1 ± 5.8%, n=4, 4 cell lines, $P<0.01$) or $p53^{+/-(ESC)}$ embryos (44/64 embryos: 69.0 ± 2.2%, n=7, 4 cell lines, $P<0.01$) (Fig. 3d). Among the normal-sized $p53^{-/-(ESC)}$ embryos, 26 of 30 (87.8 ± 9.7%, n=10, 5 cell lines) embryos were chimeras, whereas 22 of 26 displayed a relatively lower contribution of the mutant cells. Although the number of $p53^{+/-(ESC)}$ chimera (30/44 embryos, 66.9 ± 6.6%, n=7, 4 cell lines) was similar to that of $p53^{-/-(ESC)}$ chimera ($P=0.14$), the $p53^{+/-(ESC)}$ chimeras developed normally (Fig. 3c, d). The number of $p53^{+/+(ESC)}$ chimera (17/53 embryos, 36.0 ± 10.2%, n=4, 4 cell lines) was significantly smaller than that of either $p53^{+/-(ESC)}$ ($P=0.044$) or $p53^{-/-(ESC)}$ ($P=0.0081$) chimera. These results suggest that *p53* mutation enhances the chimeric contribution of ESCs and the high contribution of *p53*-null ESCs induces embryonic lethality.

To address the mechanisms by which $p53^{-/-}$ ESCs result in embryonic lethality, the behavior of $p53^{-/-}$ ESCs was followed in blastocysts incubated *in vitro*. Blastocysts were injected with 12 ESCs and incubated over night. Although $p53^{+/+1}$ ESCs remained in the blastocysts, the number decreased to 4.0 ± 0.89 cells (Fig. 3g, upper, n=5). In contrast, a significantly larger number of $p53^{C/R4}$ ESCs (13.7 ± 1.2 cells, n=7, $P<0.0001$) were detected (Fig. 3g, lower), indicating proliferation of the *p53*-null ESCs in the blastocysts. The excess proliferation may lead to a high ESC contribution, resulting in the developmental abnormalities that led to resorption of the fetuses. In fact, several of the $p53^{C/C(ESC)}$ chimeras with normal body size displayed increased number of apoptotic cells in the liver (Fig. 3h, arrowheads) and one chimera exhibited an abnormal spinal curvature (Fig. 3i, an arrow). Embryos such as these may die and undergo resorption before birth, resulting in the significant loss of neonates as shown in Figure 3d.

Morphology and global gene expression profile in $p53^{-/-}$ ESCs. The properties of $p53^{-/-}$ ESCs were examined. Venus-negative differentiated cells (Fig. 4a, left, arrowheads) survived the processes of cloning and passaging $p53^{-/-}$ Venus-positive ESCs (Fig. 4a, left, arrows), indicating that $p53^{-/-}$ differentiated cells escaped from apoptosis. Rat ESC colonies adopt a dome-shaped morphology and tend to detach from culture dishes coated with MEFs[12,15]. The $p53^{-/-}$ domed colonies were detached by pipetting and the cells were passaged after dissociation, leading to successful propagation of dome-shaped colonies; no differentiated cells were detected. (Fig. 4a, right, arrows). The morphology of the $p53^{-/-}$ lines was

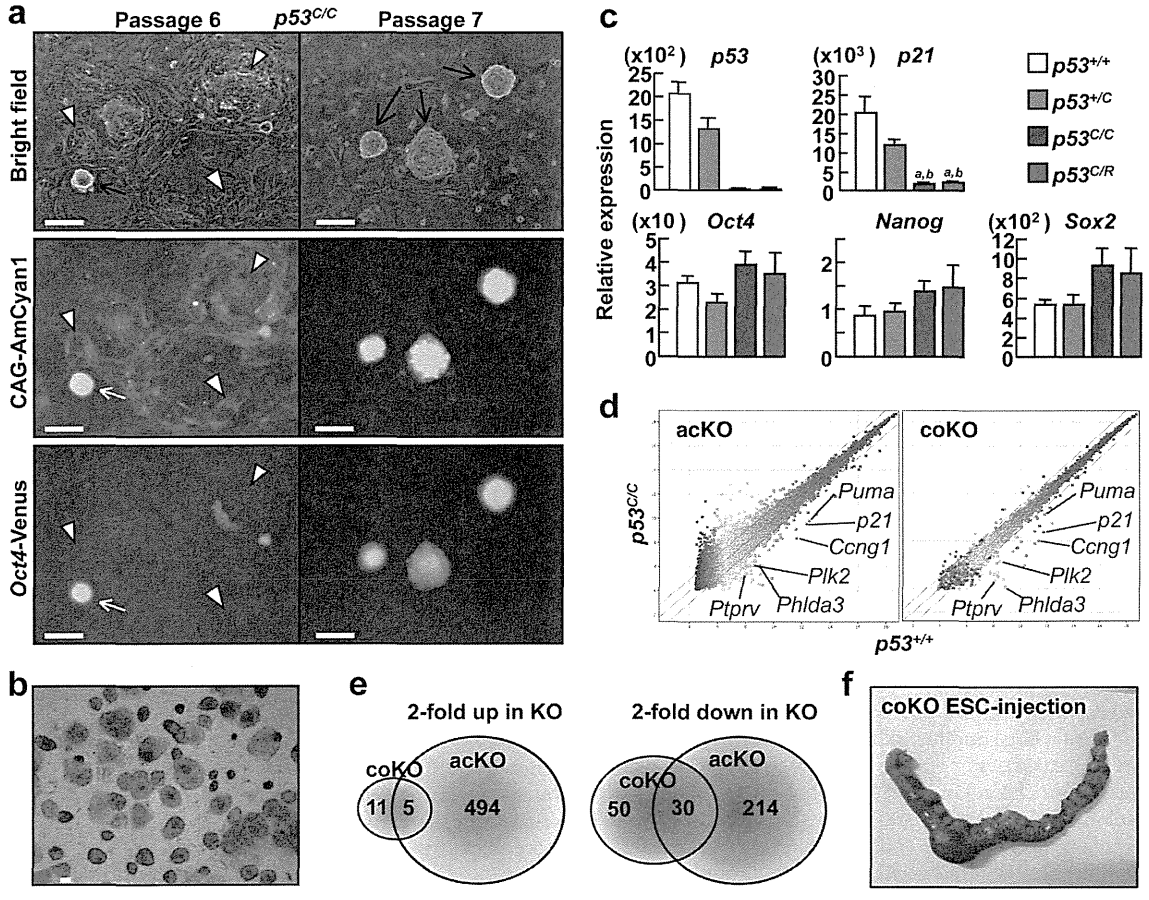

Figure 4 | Characteristics of *p53*-null ESCs. (a) A $p53^{C/C1}$ ESC clone is shown. Arrows indicate pluripotent colonies. Arrowheads indicate differentiated cells. (b) ALP staining in $p53^{C/C1}$ ESCs. (c) q-PCR analysis in *p53* mutant ESCs. Transcript levels were normalized to *Gapdh* levels. Data are the mean ± SD of one biological sample assayed in four independent experiments. *a*, $P<0.05$ versus $p53^{+/+}$; *b*, $P<0.005$ versus $p53^{+/C}$. (d) Scatter plots of global gene expression microarrays comparing $p53^{+/+}$ and $p53^{C/C}$ ESCs of an acKO (left) or coKO (right) line. The green lines delineate the boundaries of a 2-fold difference in gene expression levels. (e) Venn diagrams of the intersection between genes highly (left) or lowly (right) expressed in the coKO versus the acKO in $p53^{C/C}$ ESCs. (f) Developmental dysfunction in chimeric embryos injected with $p53^{C/C2}$ coKO ESCs at E16.0. All scale bars = 100 μm.

indistinguishable from that of $p53^{+/-}$ or $p53^{+/+}$ cells (Supplementary Fig. S3). The $p53^{C/C}$ ESCs were positive for alkaline phosphatase (ALP) activity (Fig. 4b).

The expression levels of ESC marker genes, such as *Oct4*, *Nanog* and *Sox2*, were similar in $p53^{C/C}$ and $p53^{C/R}$ ESCs compared to $p53^{+/+}$ or $p53^{+/C}$ cells, whereas loss of *p53* mRNA and parallel reduction in the mRNA level of the *p53* target gene *p21* were confirmed in mutant ESC lines (Fig. 4c). The ESC line produced by acquired gene targeting in wild-type ESCs ('acKO' ESCs) and a congenital KO ESC line derived from heterozygous intercrosses (named coKO) were analyzed to determine whether some compensatory effect occurred in the coKO line. A microarray analysis showed that the coKO line had less divergent expression compared to the acKO line (acKO vs. coKO: 494 vs. 11 genes upregulated and 214 vs. 50 genes downregulated, Fig. 4e). Venn diagrams showing the overlap in genes identified in the two KO ESC datasets identified only five upregulated and 30 downregulated genes (Fig. 4e, and see Supplementary Table S2). Many of the downregulated genes in the $p53^{C/C}$ ESCs were direct targets of *p53*, such as *Puma*, *p21*, *Ccng1*, *Plk2*, *Phlda3*, and *Ptprv* (Fig. 4d), whereas no genes for pluripotency or stemness were identified.

Chimera generation was used to investigate whether microinjection with these coKO ESCs could rescue mutant chimera development. Male ESC lines were also examined because homozygous males showed normal development. However, microinjection of both female cell lines (n=4, 2 cell lines) and male coKO ESC cell lines (n=7, 3 cell lines) produced chimeras in which embryogenesis failed, similar to the acKO chimeras (Fig. 4f and Supplementary Table S1). The fraction of full-sized embryos (15/68 embryos: 23.1 ± 4.0%, n=9, 5 cell lines) was similar to that of acKO chimeras (30/189 embryos: 20.0 ± 5.6%, n=14, 5 cell lines). These results indicate that lethality in mutant chimeras is due to abnormality of $p53^{-/-}$ ESCs.

$p53^{-/-}$ ESCs are resistant to apoptosis and differentiation. To investigate susceptibility to apoptosis, flow cytometry to detect surface exposure of Annexin V was performed in ESCs under routine culture conditions using YPAC medium [Y, Y-27632 (ROCK inhibitor); P, PD0325901 (MEK inhibitor); A, A-83-01 (TGF-β inhibitor); C, CHIR99021 (GSK3 inhibitor)][12]. A control treatment with G418 caused an increase in Annexin V-positive apoptotic cells whereas each of the *p53* genotype ESCs exhibited small population of the apoptotic cells ($p53^{+/+}$, 11.0 ± 0.25%; $p53^{+/C}$, 14.0 ± 0.30%; $p53^{C/C}$, 11.0 ± 0.49%) (Fig. 5a). Assays for colony formation and embryoid body (EB) formation were performed under differentiation culture conditions to examine the behavior of the mutant ESCs. There was no genotype-dependent difference in the numbers of undifferentiated or differentiated colonies under conditions using YPAC medium and MEFs (Fig. 5b). Under culture conditions using Y media and MEFs (inhibitors P, A and C were absent, Fig. 5c), almost no $p53^{+/+}$ undifferentiated colonies formed (1.7 ± 0.9 colonies) but some $p53^{+/C}$ colonies were observed (13.0 ± 2.1 colonies, $P<0.01$). Few differentiated colonies of either genotype were formed. In contrast, $p53^{C/C}$ cells formed a large number of both undifferentiated (56.0 ± 2.6 colonies, $P<0.0001$ vs. $p53^{+/+}$; $P<0.001$ vs. $p53^{+/C}$) and differentiated (26.3 ± 1.5 colonies, $P<0.0001$ vs. $p53^{+/+}$; $P<0.0001$ vs. $p53^{+/C}$) colonies (Fig. 5c). These results suggest that $p53^{-/-}$ ESCs strongly maintain both undifferentiated state and self-renewal capacities while the differentiated cells are protected from apoptosis, consistent with the results shown in Figure 3a. Next, colony formation was assessed under culture conditions in which ESCs weakly attach to un-coated culture dishes in the absence of MEFs. Although undifferentiated colony formation was rare in both $p53^{+/+}$ (11.3 ± 3.5) and $p53^{+/C}$ (2.0 ± 1.2) ESCs, a large number of $p53^{C/C}$ ESCs formed colonies (96.7 ± 2.8 colonies, $P<0.0001$ vs. $p53^{+/+}$; $P<0.0001$ vs. $p53^{+/C}$; Fig. 4d). In the un-coated dishes in the absence of MEFs, differentiated colonies were rarely formed from any ESC genotype. Thus, the $p53^{-/-}$ ESCs might have an increased capacity to adhere tightly to the culture dish and/or proliferate without the support of feeder cells.

When EB formation was examined, $p53^{+/+}$ EBs formed by day 3 underwent apoptosis over time in culture, resulting in few EBs remaining by day 7 relative to day 3. In addition, Venus fluorescence was completely lost in these cells (Fig. 5e, left). In contrast, $p53^{C/C}$ EBs were large in size and number, and maintained Venus fluorescence (Fig. 5e, right). The number of cells in $p53^{C/C}$ EBs (3.25×10^5) was significantly larger than cell number in $p53^{+/+}$ EBs (1.00×10^3, $P<0.01$) or $p53^{+/C}$ EBs (2.47×10^4, $P<0.01$). Moreover, these data indicate that $p53^{C/C}$ EBs actively proliferated because the cell number increased from 2.5×10^5 at day 0 to 3.25×10^5 by day 7 (Fig. 5f). This result suggests that $p53^{C/C}$ cells are able to proliferate even in the absence of cell attachment. $p53^{+/C}$ EBs showed an intermediate phenotype with significant differences from the other genotypes ($P<0.01$ vs. $p53^{+/+}$, $P<0.01$ vs. $p53^{C/C}$).

Chromosomal instability in $p53^{-/-}$ cells. Next, karyotype analysis was performed in $p53^{-/-}$ cells. Although $p53^{+/C}$ ESCs maintained a normal karyotype 42,XX,[20], one $p53^{C/R2}$ ESC clone exhibited abnormal karyotype 42,XX,add(15)(q22)[20] (Fig. 6a, red square and arrow). Moreover, once the $p53^{C/R2}$ ESC clone differentiated under EB forming culture conditions for two weeks (Fig. 6b), an additional chromosomal aberration, 41,X,-X,add(15)(q22)[20], was found in all cells analyzed (Fig. 6a, blue square). In a $p53^{C/C1}$ ESC clone, ESCs did not have an abnormal karyotype (42,XX[20]). However, cells derived from the $p53^{C/C1(ESC)}$ chimera in E14.0 rats displayed various chromosomal aberrations, such as 42,XX,add(1)(q52)[1], 42,XX,add(3)(p12) [1], 43,XX,+16[1] or 42,X,-X,+mar[1]. In cell cultures, $p53^{+/+}$ cells derived from a recipient blastocyst were eliminated, resulting in occupation by $p53^{C/C1}$ cells with AmCyan1 expression (Fig. 6c).

These findings demonstrate that $p53^{-/-}$ ESCs exhibit several features of abnormalities, such as blockage of differentiation, induction of chromosomal instability, and escape from apoptosis, which are facilitated when the cells differentiate. Thus, p53 is indispensable for embryonic development in the mutant chimeric models (Fig. 1f) but dispensable in the homozygous models due to bypassing an ESC state (Fig. 1e).

Discussion

Here, two distinct strategies were used to generate *p53* KO rats: conventionally generated homozygous KO and ESC-based mutant chimeras. In the homozyogous KO rats, NTDs such as exencephaly and spina bifida were observed. This is the first NTD model created in genetically modified rats. Previously, a 50% reduction in the number of females relative to males at weaning was observed in *p53* homozygous KO mice[17]. In contrast, in the present study, a 96% reduction in the number of *p53* homozygous KO female rats surviving to weaning relative to homozygous KO males was observed (Table 1). In rats, exencephaly occurred in a large fraction of the homozygous KO females (55%; Table 1), whereas only 8–16% of homozygous KO female mouse embryos exhibited exencephaly[17,18]. The survival ratio and spina bifida phenotype observed in these exencephalic rat embryos suggests that this species exhibits more severe phenotypes than mice. We hypothesize that rats are more sensitive to the stress of DNA damage than mice. Consistent with this observation, rat ESCs are more sensitive to differentiation signals than mouse ESCs, which is one reason why rat ESCs were not established until 2008. Mouse ESCs are very stable compared to other species. In mouse, successful chimera contribution and germline transmission using *p53*-null mouse iPSCs has been reported[24,25]. These results were unexpected, considering the vast amount of data regarding the effects of p53 on cell cycle arrest, apoptosis, and DNA

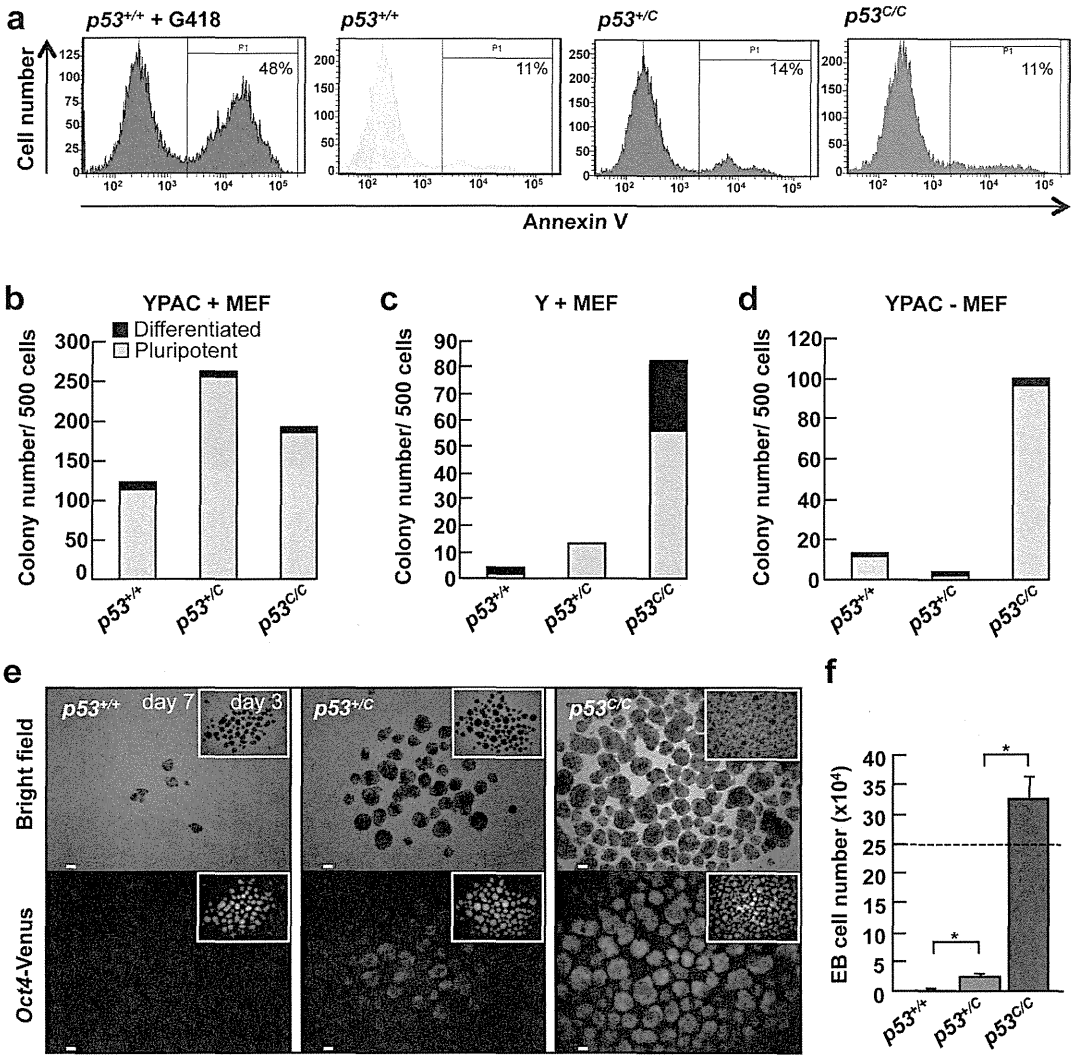

Figure 5 | Colony and EB formation assays under differentiating conditions. (a) Flow cytometry analysis. Annexin V-Cy5 was used to detect apoptotic cells (n=3). (b–d) Colony formation assay. Five hundred cells were cultured under normal conditions (YPAC+MEF; b), differentiation conditions (Y+MEF; c), or apoptosis-inducing conditions (YPAC-MEF; d). A green or black bar indicates pluripotent or differentiated colony number, respectively (n=3 or 4). (e, f) EB formation assay. EBs were formed from 2.5×10^5 cells (f, dotted line). Seven days after incubation without inhibitors, the cell number was counted (f, n=3). Insets (e) indicate EBs at day 3. *, $P < 0.01$. All scale bars = 100 μm.

repair. In contrast, in the present study, mutant chimeras generated with rat ESCs demonstrated a clear phenotype of embryonic lethality, consistent with the data presented here showing the down-regulation of *p53* target genes, inhibition of apoptosis and differentiation, and increase in chromosomal instability in *p53*-null rat ESCs or ESC-derived cells.

The rat is considered to be a better model than the mouse for many complex disorders that are common in humans[36] and is currently the primary animal model in many preclinical tests, especially those related to cardiovascular disease, diabetes, breast cancer, chronic inflammatory diseases, and age-related diseases[20]. Genetically modified rats are valuable platforms for the study of human physiology and disease. For example, in comparison to transgenic mice, transgenic rat models of Huntington disease not only present a more typical adult patient pathology but are also more suitable for *in vivo* metabolic and structural imaging[20,37]. In addition, *Apc* knockout mice develop tumors primarily in the small intestine, whereas both humans and rats develop colon cancer as a result of the *Apc* mutation[38]. These observations support the inconsistent phenotype of *p53* mutant chimeras between rats and mice, as shown in the present work, and suggest the importance of generating genetically modified rats to find novel gene functions.

In this study, the differences in the phenotypes of the *p53* homozygous and mutant chimeric rat models were striking. Secondary mutations are accumulated in the mutant ESCs under *in vitro* culture conditions and in the differentiating cells during embryogenesis (Fig. 6). These aberrant cells are resistant to apoptosis due to *p53* deficiency, which might lead to lethality of the mutant chimeras. These observations reflect the fact that a major p53 function is to be the "guardian of the genome". Thus, the mutant chimeric strategy may prove useful in identifying authentic and/or novel gene functions. Finally, the present study demonstrated that mutant chimeric models can be generated within one month, circumventing both the risks associated with producing successful germline transmission as well as the time frame required for breeding both chimeras and heterozygous animals. In the mutant chimeric method, double or triple gene knockouts can be generated in a few months. These new combination strategies using embryonic stem cells, the mutant

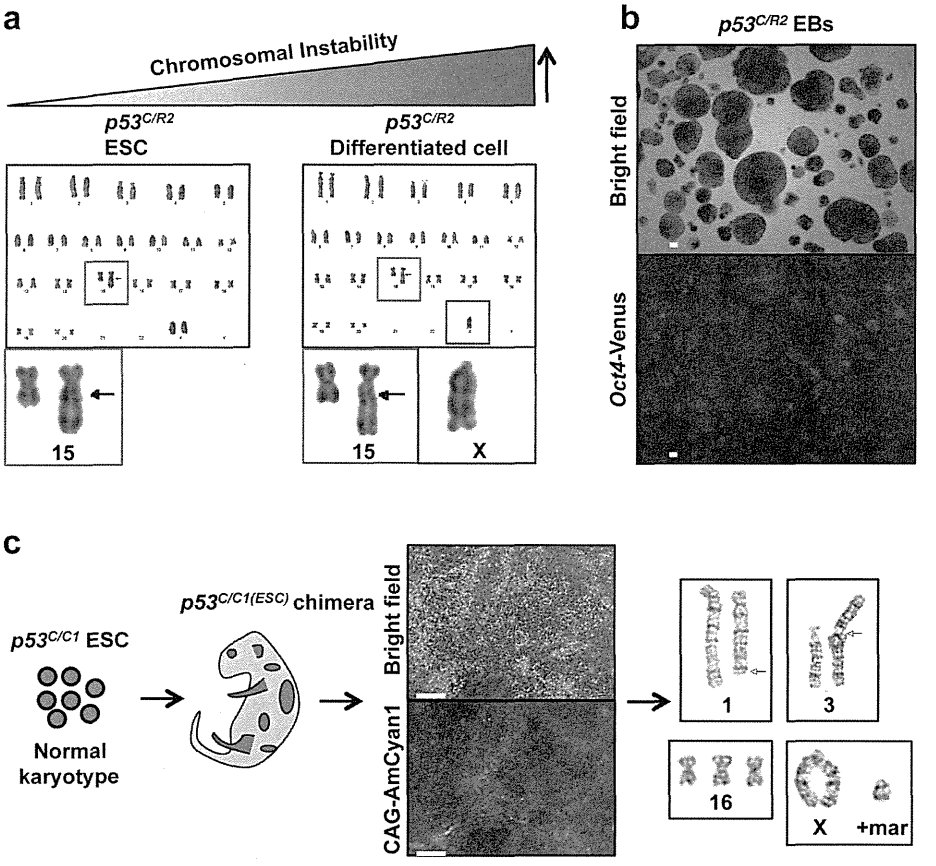

Figure 6 | Chromosomal instability in *p53*-null cells. (a) Cytogenetic analysis by G-band staining in $p53^{C/R2}$ ESCs and EB-derived differentiated $p53^{C/R2}$ cells. Abnormal chromosomes were indicated by red and blue squares. (b) Differentiated $p53^{C/R2}$ EBs lacking Venus fluorescence. (c) Aberrant chromosomes were observed in cells derived from a $p53^{C/C1(ESC)}$ chimera at E14.0.

chimeric method, and rats instead of mice will provide great insight into the novel functions of a large number of genes. The first example, shown here by deleting the *p53* gene, provided new, substantial evidence demonstrating that p53 functions not only as the "guardian of the genome", but also as the "guardian of the embryogenesis".

Methods

Media, feeder cells, animals, and primers. The YPAC medium was prepared by the addition of the following inhibitors: 10 μM Y-27632 (WAKO), 1 μM PD0325901 (Axon Medchem), 0.5 μM A-83-01 (TOCRIS), and 3 μM CHIR99021 (Axon Medchem) to a basic medium. The basic medium was composed of DMEM (including 110 mg/L sodium pyruvate and 200 mM GlutaMAX, GIBCO), 20% FBS (ES Cell Qualified Fetal Bovine Serum, Lot No. 1204059, GIBCO), 0.1 mM 2-mercaptoethanol (SIGMA), 1% nonessential amino acid stock (GIBCO), and 1× antibiotic antimycotic (GIBCO). Mitomycin C-treated MEFs resistant to neomycin (Millipore) were used as feeders and maintained in 10% FBS DMEM (Lot No. SFB30-1502, EQUITECH-BIO, INC.) with 1× antibiotic antimycotic. Animal experiments were performed in compliance with the guidelines of the Institute for Laboratory Animal Research, National Cancer Center Research Institute. These studies were approved by National Cancer Center Research Institute. All primer sequences are listed in Supplementary Table 3.

Generation of *Oct4*-Venus Tg rats and ESCs. *Oct4*-Venus Tg rats of the Wistar strain were generated via germline transmission of an *Oct4*-Venus ESC clone in the same manner described previously[12]. The *Oct4*-Venus ESC line derived from the Long-Evans Agouti (LEA) strain was generated in an earlier study[12].

Establishment of rat ES cells from blastocysts. Rat blastocysts were gently flushed out from the uteri of E4.5 or E5.0 pregnant rats with a basic ES medium. After removal of the zona with acid Tyrode's solution (Ark Resource Co., Ltd.), whole blastocysts were plated onto 6-well plates and cultured on MEFs in basic ES medium with or without YPAC. After approximately 7 days, the blastocyst outgrowths were cut into pieces and replated under the same YPAC conditions. Emerging ESC colonies were then dissociated with Accutase (Innovative Cell Technologies, Inc.) and expanded. Domed and floated ESC colonies were detached from MEFs by pipetting, followed by routinely passaging every 3–4 days under MEF-YPAC conditions.

ZFN constructs and targeting plasmids. Custom-designed ZFN plasmids and ZFN-encoding mRNA for the rat *p53* gene were purchased from Sigma-Aldrich. The design, cloning, and validation of the ZFNs were performed by Sigma-Aldrich. The ZFN pair recognizing exon 4 of the *p53* gene was 5′: TTCTCCAGTCTTCCTCCAG, 3′: ATTCTGGTAAGGAGCCGG. The targeting donor was composed of the CAG-AmCyan1-IRES-Neo-pA or CAG-tdTomato-IRES-Neo-pA cassette with short homology 5′ (736 bp) and 3′ (711 bp) arms. These homology arms were amplified from rat genomic DNA using the KOD Ver.2 DNA polymerase PCR system (Toyobo). The sequences of these primers are listed in Supplementary Table S3. Both arms were set at several base pairs from a ZFN-induced cleavage site.

Introduction of the targeting vector and ZFNs into LEA rat ESCs and generation of *p53* heterozygous rats. To disrupt exon 4 of the *p53* gene, 5 μg of ZFN-encoding mRNAs and 10 μg of a targeting plasmid (5′arm-CAG-AmCyan1-IRES-Neo-pA-3′arm cassette) were co-transfected into 6.5×10^5 of *Oct4*-Venus ESCs derived from a LEA female strain at passage 5 with a Mouse ESC Nucleofector Kit (Amaxa Inc.). The cells were plated on MEFs in YPAC medium with 2% Matrigel (BD Biosciences) to keep the ESC colonies adhered to the MEFs. One day after nucleofection, geneticin was added to the YPAC medium at 0.2 μg/ml. Eleven days after nucleofection, geneticin-resistant colonies were selected using handmade capillaries and expanded. Picking and expanding seven colonies provided four (57%) heterozygous ($p53^{+/C}$) clones and two (29%) homozygous clones harboring both knock-in and frame shift mutation alleles ($p53^{C/Z}$) (Supplementary Fig. S1a). The ZFN-induced frame shift mutation was identified by band shift in PCR analysis (Supplementary Fig. S1a, No. 6 clone, asterisk) and sequence analysis (Supplementary Fig. S1c) or using a SURVEYOR Mutation Detection Kit (Supplementary Fig. S1b, No. 8 clone). A $p53^{+/C}$ ESC clone was used for microinjection, resulting in the generation of $p53^{+/C}$ rats through chimeric germline transmission.

Introduction of the targeting vector and ZFNs into Wistar rat ESCs. For nucleofection, 10 μg of a targeting plasmid (5′arm-CAG-AmCyan1-IRES-Neo-pA-3′arm

cassette) and 5 μg of ZFN-encoding mRNAs were co-transfected into 4.5×10^6 of *Oct4*-Venus ESCs (Wistar) at passage 3. As a control experiment, 10 μg of the targeting plasmid without ZFNs was transfected into 4.5×10^6 of *Oct4*-Venus ESCs at passage 3. One out of 46 (2.2%) clones was $p53^{C/C}$, while seven of 46 (15%) clones were $p53^{C/Z}$. A sequence data revealed an 8-bp deletion in the $p53^{C/Z1}$ clone (Figure S2B). This ZFN-induced small deletion was also confirmed by a downward band shift (indicated by asterisks in Supplementary Fig. S2a). As a control experiment, the targeting vector alone was introduced without ZFN. Although 14 geneticin-resistant colonies appeared, they did not achieve homologous recombination (Supplementary Fig. S2a, lane 5). Knockout clones were also produced using a 2nd-step recombination by introducing the 10 μg of targeting plasmid (5′arm-CAG-tdTomato-IRES-Neo-pA-3′arm cassette) and 5 μg of ZFN-encoding mRNAs into 2.5×10^6 cells of a $p53^{+/C3}$ ESC clone at passage 9 (Fig. 6). Eight red fluorescence (tdTomato)-positive clones were chosen without geneticin selection, and successful homologous recombination was achieved in three of these (38%, $p53^{C/R}$; Supplementary Fig. S2c).

Surveyor nuclease (Cel-I) assay. A ZFN target locus was amplified by PCR (35 cycles: 10 s denaturing at 98°C, 30 s annealing at 62°C and 1 min elongation at 72°C) using primers 1 and 5 (Fig. 6 and Supplementary Table S3). The Cel-I assay was carried out following the manufacturer's protocol (TRANSGENOMIC, Inc.).

ALP staining, immunohistochemistry (IHC) and Annexin V-apoptosis assay. Cells were fixed in 4% paraformaldehyde. ALP staining was performed with the Vector Blue substrate (Vector Labs) according to the manufacturer's instructions. Formalin-fixed and paraffin-embedded slides were stained with hematoxylin and eosin or used for IHC. Antigen retrieval was performed by autoclave in a sodium citrate buffer. The slides were incubated with Sox2 (BioLegend, 1 : 200) or Cleaved Caspase-3 (Cell Signaling, 1/1000) primary antibody at 4°C overnight. The next day, after washing, the samples were incubated with horseradish peroxidase-conjugated secondary antibody for 1 h. They were then washed and incubated with 3,3′-diaminobenzidine tetrahydrochloride DAB (Thermo Scientific). An assay for apoptotic ESCs was performed using Annexin V-Cy5 following the manufacturer's protocol (BioVision). Pluripotent ESC colonies were solely harvested and dissociated with Accutase, followed by incubating $1–5 \times 10^5$ cells with the Annexin V-Cy5 for 5 min in the dark.

Q-PCR analysis. Total RNA was isolated using ISOGEN (Nippongene). cDNA was synthesized with 2 μg of the total RNA using Super Script III RT (Invitrogen) and oligo-dT primer (Invitrogen). cDNAs were used for PCR using Platinum SYBR Green qPCR SuperMix UDG (Invitrogen). Optimization of the q-PCR reaction was performed according to the manufacturer's instructions (PE Applied Biosystems, Tokyo, Japan). All quantitations were normalized to an endogenous control *GAPDH*.

Microarray analysis. A one-color microarray-based gene expression analysis system (Agilent Technologies) using SurePrint G3 Rat GE 8×60 K Kit containing 30507 probes (26930 genes) was used following the manufacturer's instructions.

EB formation. After ES cells were dissociated into single cells using Accutase, 5×10^5 cells were cultured in PAC medium. After overnight incubation, the EB contained media were separated and cultured in media with or without PAC on a low cell-binding dish (NUNC). After 7 days of incubation, the cell number of EBs was counted after dissociation with Accutase.

Chimera production. In all blastocyst injection experiments, 12 ESCs were injected into E4.5 blastocysts. YPAC or PAC inhibitors were constantly included in media during both microinjection and blastocyst incubation. ESC-injected blastocysts were transferred to E3.5 pseudo-pregnant rats. The contribution of ESCs to the resulting chimeras was determined by the appearance of coat-color or fluorescence.

Karyotype analyses in $p53^{-/-}$ cells. G-band staining was performed in cultured cells from embryos, ESCs, or ESC-derived differentiated cells. Head of E14.0 chimeric embryo was dissociated with Accutase and karyotype analysis was examined in the cells at passage 4. $p53^{C/R2}$ ESCs at five passages after the generation of the gene-targeted null mutation or EB-derived differentiated $p53^{C/R2}$ cells at seven passages were analyzed. EBs were formed at passage 5 and cultured for 2 weeks, followed by two passages to expand the cells. The differentiated state was confirmed by a loss of *Oct4*-Venus expression, as well as by the cell morphology.

Statistical analysis. Results are given as the mean ± SD. Statistical analysis was conducted using Student *t*-tests. $P < 0.05$ was considered significant.

1. Cozzi, J. *et al.* Pronuclear DNA injection for the production of transgenic rats. *Methods Mol. Biol.* **561**, 73–88 (2009).
2. Dann, C. T., Alvarado, A. L., Hammer, R. E. & Garbers, D. L. Heritable and stable gene knockdown in rats. *Proc. Natl. Acad. Sci. U S A.* **103**, 11246–11251 (2006).
3. Zan, Y. *et al.* Production of knockout rats using ENU mutagenesis and a yeast-based screening assay. *Nat. Biotechnol.* **21**, 645–651 (2003).
4. van Boxtel, R., Gould, M. N., Cuppen, E. & Smits, B. M. ENU mutagenesis to generate genetically modified rat models. *Methods Mol. Biol.* **597**, 151–167 (2010).
5. Kitada, K. *et al.* Transposon-tagged mutagenesis in the rat. *Nat. Methods* **4**, 131–133 (2007).
6. Kitada, K., Keng, V. W., Takeda, J. & Horie, K. Generating mutant rats using the Sleeping Beauty transposon system. *Methods* **49**, 236–242 (2009).
7. Izsvák, Z. *et al.* Generating knockout rats by transposon mutagenesis in spermatogonial stem cells. *Nat. Methods* **7**, 443–445 (2010).
8. Geurts, A. M. *et al.* Knockout rats via embryo microinjection of zinc-finger nucleases. *Science* **325**, 433 (2009).
9. Mashimo, T. *et al.* Generation of knockout rats with X-linked severe combined immunodeficiency (X-SCID) using zinc-finger nucleases. *PLoS One* **5**, e8870 (2010).
10. Buehr, M. *et al.* Capture of authentic embryonic stem cells from rat blastocysts. *Cell* **135**, 1287–1298 (2008).
11. Li, P. *et al.* Germline competent embryonic stem cells derived from rat blastocysts. *Cell* **135**, 1299–1310 (2008).
12. Kawamata, M. & Ochiya, T. Generation of genetically modified rats from embryonic stem cells. *Proc. Natl. Acad. Sci. USA* **107**, 14223–14228 (2010).
13. Hamanaka, S. *et al.* Generation of germline-competent rat induced pluripotent stem cells. *PLoS One* **6**, e22008 (2011).
14. Hirabayashi, M. *et al.* Rat transgenesis via embryonic stem cells electroporated with the Kusabira-orange gene. *Mol. Reprod. Dev.* **77**, 474 (2010).
15. Tong, C., Li, P., Wu, N. L., Yan, Y. & Ying, Q. L. Production of p53 gene knockout rats by homologous recombination in embryonic stem cells. *Nature* **467**, 211–213 (2010).
16. Donehower, L. A. *et al.* Mice deficient for p53 are developmentally normal but susceptible to spontaneous tumours. *Nature* **356**, 215–221 (1992).
17. Armstrong, J. F., Kaufman, M. H., Harrison, D. J. & Clarke, A. R. High-frequency developmental abnormalities in p53-deficient mice. *Curr. Biol.* **5**, 931–936 (1995).
18. Sah, V. P. *et al.* A subset of p53-deficient embryos exhibit exencephaly. *Nat. Genet.* **10**, 175–180 (1995).
19. Donehower, L. A. & Lozano, G. 20 years studying p53 functions in genetically engineered mice. *Nat. Rev. Cancer* **9**, 831–841 (2009).
20. Huang, G. *et al.* Beyond knockout rats: new insights into finer genome manipulation in rats. *Cell Cycle* **10**, 1059–1066 (2011).
21. van Boxtel, R. *et al.* Homozygous and heterozygous p53 knockout rats develop metastasizing sarcomas with high frequency. *Am. J. Pathol.* **179**, 1616–1622 (2011).
22. Puzio-Kuter, A. M. & Levine, A. J. Stem cell biology meets p53. *Nat. Biotechnol.* **27**, 914–915 (2009).
23. Lin, T. *et al.* p53 induces differentiation of mouse embryonic stem cells by suppressing Nanog expression. *Nat. Cell Biol.* **7**, 165–171 (2005).
24. Hong *et al.* Suppression of induced pluripotent stem cell generation by the p53–p21 pathway. *Nature* **460**, 1132–1135 (2009).
25. Marion *et al.* A p53-mediated DNA damage response limits reprogramming to ensure iPS cell genomic integrity. *Nature* **460**, 1149–1153 (2009).
26. Kawamata, M. & Ochiya, T. Establishment of embryonic stem cells from rat blastocysts. *Methods Mol. Biol.* **597**, 169–177 (2010).
27. Kawamata, M. & Ochiya, T. Gene-manipulated embryonic stem cells for rat transgenesis. *Cell Mol. Life Sci.* **68**, 1911–1915 (2011).
28. Hosako, H. *et al.* The roles of p53 and p21 in normal development and hyperthermia-induced malformations. *Birth Defects Res. B Dev. Reprod. Toxicol.* **86**, 40–47 (2009).
29. Chen, X. *et al.* Sex difference in neural tube defects in p53-null mice is caused by differences in the complement of X not Y genes. *Dev. Neurobiol.* **68**, 265–273 (2008).
30. Takemoto, T. *et al.* Tbx6-dependent Sox2 regulation determines neural or mesodermal fate in axial stem cells. *Nature* **470**, 394–398 (2011).
31. Miyagi, S. *et al.* The Sox2 regulatory region 2 functions as a neural stem cell-specific enhancer in the telencephalon. *J. Biol. Chem.* **281**, 13374–13381 (2006).
32. Hockemeyer, D. *et al.* Efficient targeting of expressed and silent genes in human ESCs and iPSCs using zinc-finger nucleases. *Nat. Biotechnol.* **27**, 851–857 (2009).
33. Soldner, F. *et al.* Generation of Isogenic Pluripotent Stem Cells Differing Exclusively at Two Early Onset Parkinson Point Mutations. *Cell* **146**, 318–331 (2011).
34. Meyer, M., de Angelis, M. H., Wurst, W. & Kühn, R. Gene targeting by homologous recombination in mouse zygotes mediated by zinc-finger nucleases. *Proc. Natl. Acad. Sci. USA* **107**, 15022–15026 (2010).
35. Cui, X. *et al.* Targeted integration in rat and mouse embryos with zinc-finger nucleases. *Nat. Biotechnol.* **29**, 64–67 (2011).
36. Abbott, A. Return to the rat. *Nature* **460**, 788 (2009).
37. von Horsten, S. *et al.* Transgenic rat model of Huntington's disease. *Hum. Mol. Genet.* **12**, 617–24 (2003).
38. Amos-Landgraf, J. M. *et al.* A target-selected Apc-mutant rat kindred enhances the modeling of familial human colon cancer. *Proc. Natl. Acad. Sci. U.S.A.* **104**, 4036–41 (2007).

Acknowledgements

We thank F. Takeshita, T. Katsuda, K. Hagiwara, Y. Yoshioka, R. Takahashi, N. Kosaka, H. Tsuda, H. Sasaki and Y. Tamai for their technical advice. This work is supported by a Grant-in-Aid from the Third-Term Comprehensive 10-Year Strategy for Cancer Control.

Author contributions

M.K. designed and performed experiments. M.K. and T.O. wrote the manuscript. T.O. supervised the project.

Additional information

Supplementary information accompanies this paper at http://www.nature.com/scientificreports

Competing financial interests: The authors declare no competing financial interests.

How to cite this article: Kawamata, M. & Ochiya, T. Two distinct knockout approaches highlight a critical role for p53 in rat development. *Sci. Rep.* **2**, 945; DOI:10.1038/srep00945 (2012).